FOREST OWNERS ASSOCIATION

Forest Owners Association
PO Box 1127
Rotorua 3040
Ph: +64 7 921 1883

Programme: Sustainable Intensification

Use of Remotely Sensed Data for Forest Inventory Purposes in Tairua Forest

Authors:
Jonathan Dash, David Pont, Michael S Watt

Research Provider:

SCION
Next generation biomaterials

Task No: F70004
Milestone Number: RA 2.1.7
Report No. GCFF-T001

Date: March 2014

forestgrowers
levy trust inc

TABLE OF CONTENTS

EXECUTIVE SUMMARY

Using LiDAR data obtained for Tairua Forest, the objectives of this research were to (1) determine the number of plots by stand required to obtain a PLE of 10% on TRV, (2) use LiDAR data to develop maps describing site index and age of final thinning, (3) evaluate whether LiDAR data can be used to accurately derive estimates of 300 Index, (4) validate the accuracy of tree counting using both ground and image calibration methods, and (5) for MRI, establish if a stem list can be derived from LiDAR that allows generation of a yield table.

Objective 1: A methodology was developed to determine the required sample size to meet a specific allowable error from aerial LiDAR data. Results show that this methodology can be used to markedly reduce costs in Tairua Forest through ensuring that stand level plot intensity is well matched to variation within the stand. Implementation of the k nearest neighbour methodology (kNN) within Tairua Forest shows that even greater cost savings can be made through implementation of this method to predict TRV.

Objectives 2 and 3: Methodologies are described that allow determination of site index and 300 Index throughout Tairua Forest from LiDAR data. Estimates of site index were used to develop a map of the final thinning age. The kNN methodology was used to produce a map of 300 Index from LiDAR data and plot information.

Objective 4: Tree counting was accurately undertaken using both the ground and image calibration methods, which confirms earlier results from a case study at Kaingaroa despite lower pulse density and more complex terrain. Count methods using ground calibration deliver 6% RMSE, while image-based calibration results in RMSE of 11%. The ground calibration method delivers an improvement of 1.2% in RMSE over use of ground plots alone.

Objective 5: Individual tree metrics, delineated from the LiDAR data, were well correlated to both tree height and diameter at breast height (DBH), with respective R^2 for the best metrics of 0.92 and 0.83. However, the diameter distributions generated by the model did not closely match those observed in ground measurements, the model over-estimating the numbers of trees at the low and high ends of the DBH distribution. Future work should attempt to solve the problem of accurately locating individual trees on the ground. The ability to spatially match single tree ground and crown measures will allow more meaningful evaluation of crown metrics for estimation of individual tree attributes such as DBH.

INTRODUCTION

The objectives addressed in this study were to:

1. for PHI, determine the number of plots required to achieve a PLE of 10% on TRV when LiDAR is available;
2. use LiDAR data to develop maps describing site index and age of final thinning;
3. evaluate whether LiDAR data can be used to accurately derive estimates of 300 Index;
4. validate the accuracy of tree counting using both ground and image calibration methods; and
5. for MRI, establish if a stem list can be derived from LiDAR that allows generation of a yield table.

Aerial LiDAR Sampling

The light detection and ranging (LiDAR) data used in this analysis were derived from airborne LiDAR scanning of the study area. LiDAR acquisition was carried out by Aerial Surveys Ltd using a fixed wing aircraft on 7-9 July 2012. An Optech ALTM 3100EA scanner was used at a flying height of 1650 m above mean ground level, acquiring data at a designed pulse density of two per square metre with a 50% swath overlap. The point cloud data were then classified into ground, first and, intermediate returns using automated routines tailored to the project land cover and terrain. The subsequent steps were undertaken using TerraSolid LiDAR processing software module TerraScan. Manual editing of the LiDAR point cloud data was undertaken to increase the quality of the automatically classified ground and above-ground point dataset. This editing involved visually checking over the data and changing the classification of points into and out of the ground point dataset. Aerial Surveys reported a resulting mean pulse density of 2.38 points per square metre per swath.

The FUSION LiDAR analysis software product was used to produce various statistical parameters describing the LiDAR dataset in terms of point elevations and intensity. These statistical parameters (Table 1) served as candidates for the predictor variables used in this analysis. These variables would be used in both the target and the reference dataset.

Table 1. Summary of the area based LiDAR metrics developed for the study area.

Metric	Description
Heights	Distribution of all returns
Percentile heights	Distribution by decile of all returns
Intensity	Distribution of all return intensities
Percentile intensity	Distribution by decile of all return intensities
Canopy cover	Percentage of returns above a specified height (e.g. 0.5 m, 2 m, mean return height…)

Ground Sampling

The ground sampling data available for this project are summarised below. Due to the complex and multi-objective nature of the project, the field measurement was reasonably comprehensive. Where required, additional detail is provided in later sections of the report.

1. **Mensuration Ground Plots**
- A total of 99 mensuration ground (MG) plots were established across the forest during January 2013.

- All plots were allocated to stands <u>older than 10 years</u>. The majority of these plots (66%) were to be allocated in stands older than 20 years.
- An accurate location was derived for each plot using differential GPS. Plot size was 0.06 ha.
- Plot measurements associated with each age class are given in Table 2

Table 2. Information required for each of the stand ages sampled

Stand age	Data collected
10 to 20 years	Stocking, height, diameter,
20 years on	Stocking, height, diameter, full cruise

2. PHI Plots

- Existing PHI plots measured in 2012 and 2013 in stands at ages 20 and above can be utilised in this study by re-locating plot centres accurately with high-grade GPS. Approximately 30 stands (over 300 plots) were assessed in May-June each year. A selection of these stands will be made to provide data for analyses.
- PHI plots from an additional five stands provided a total of 10 PHI stands for objective 1 (PLE on TRV).

3. Additional Sampling

- The existing MG and PHI plots largely meet the needs of objectives 1, 2 and 3. For objectives 4 and 5, additional sampling is required. A set of five stands was selected from each of three age classes. The three age classes were: silvicultural phase (S); mid-rotation (M); and pre-harvest (P), identified as S, M and P respectively. An additional four pre-harvest stands were also selected (identified X), but two were felled before ground measurement, giving a total of 17 stands assessed (see Table 3).

Table 3. Characteristics of stands and sample plots for additional sampling. Base matrix of 15 stands, with two additional PHI stands for Objective 1.

Age class	Stand	Age (y)	SPH	Stand area (ha)	Area assessed (ha)	Plot area (ha)	Tally plots
S1	118_2	12.56	1366.67	32.70	10.20	0.01	10
S2	126_4	13.56	550.00	85.08	20.90	0.04	21
S3	135_3	12.56	416.67	34.93	27.30	0.05	14
S4	117_5	11.56	800.00	43.83	35.10	0.02	23
S5	84_4	13.54	383.33	8.31	8.20	0.05	10
M1	24_3	20.56	516.67	27.62	27.60	0.04	18
M2	31_2	21.56	550.00	9.39	9.40	0.04	9
M3	31_4	21.56	466.67	45.97	46.00	0.04	23
M4	35_4	18.59	433.33	41.51	31.80	0.05	21
M5	145_6	20.56	416.67	21.08	21.10	0.05	21
P1	59_2	25.58	400.00	46.57	46.57	0.05	14
P2	64_3	24.54	383.33	13.03	13.03	0.05	5
P3	98_8	24.56	383.33	25.25	25.25	0.06	13
P4	64_2	24.54	433.33	27.23	27.23	0.05	9
P5	98_9	24.56	350.00	3.97	3.97	0.06	2
X2	29_4	25.56	350.00	28.93	28.93	0.06	16
X3	65_4	24.54	400.00	13.92	13.92	0.04	15

4. Tree Delineation

- Objectives 4 and 5 require delineation of individual trees from LiDAR-derived CHM images.
- This requires ground tally plots to calibrate the delineation system, at a nominal sampling intensity of one plot per hectare located on a grid with random origin and orientation.

- Stand selection was restricted to stands sized above 6 ha to ensure the number of tally plots is adequate for calibration
- Tally plots were sized (using SPH from stand records) to obtain a nominal 20 trees per plot. Each calibration tally plot required a location, assessed by collecting 500 points with a high-grade GPS, a tree count (tally) and a crown visibility assessment for each tree.
- Edge plots were handled using the Mapped Plot method (any part of the plot falling inside the stand is assessed) with reference in the field to maps clearly showing the mapped plot and stand boundaries.
- Objective 4 required high intensity tally plots to establish reference counts. These were located by doubling the sampling rate required for calibrating tree detection.
- Objective 5 required tree DBH data to be collected from plots at a lower sampling intensity. These data were collected within tally plots selected by halving the sample rate required for calibrating tree detection.

5. Tree Counting
- A new tree counting methodology was evaluated in six stands, two in each of the three age classes, to quantify accuracy on a steeper terrain forest using LiDAR taken at a pulse density of two pulses m^{-2}.
- Visual review of stand CHM images across the target range of ages (above 10 years) indicated that the images derived from this LiDAR dataset have sufficient resolution to carry out tree counting.
- Testing of tree counts required high intensity tally plots to establish an accurate estimate of stand tree count. This was achieved by adding additional tally plots in those stands at the nominal rate of one plot per hectare (total number of plots double the intensity of calibration plots). In the additional tally plots a tree count is adequate, crown visibility is not required.
- For the P age class, existing PHI plots were used as the base calibration plots, with additional tally plots added to achieve the required high intensity sample for count testing.

6. MRI Stem List
- The ability to generate a stem list was evaluated in five mid-rotation stands across the range of slenderness.
- Creating a stem list requires methods to estimate individual tree height and DBH. It was proposed to use plot mean tree height from the MG plots to derive a forest-level model fitted to plot mean CHM tree height. For DBH, stand-level models were fitted to plot mean DBH measurements and plot mean CHM crown diameters. This required measurement of DBH of all trees in low intensity plots for mid-rotation (M) stands.
- Plots for DBH measurement were a sub-selection (approximately half) of the calibration tally plots in the stand (one plot per 2 ha).

7. Forest Company Data
Forest information records were made available for this project by the forest manager:
- Stand records for the 99 stands sampled with MG plots, including MTH, SPH, BA, and silvicultural history (for 300 Index).
- PHI data for 2012 and 2013. Plot GPS locations and maps if they were available in pdf form. Plot data in csv files, giving field measurements: DBH, height, stem description.

Objective 1

For pre-harvest inventory, determine the number of plots required to achieve a PLE of 10% on TRV when LiDAR is available

Methods and Results

This section addresses Objective 1 of the Tairua work plan. This objective addresses how best to use pre-existing LiDAR data to inform sample size determination where the sampling objective is to achieve a Probable Limit of Error (PLE) of 10% for a given stand in the forest. The forest manager employs simple random sampling, and this analysis makes reference to this sampling strategy in the first instance.

In practice the estimation of sample size for a forest inventory usually follows some simple rule of thumb, such as a sampling fraction of 10% by area. These simplistic approaches lead to estimates that are more precise than required, and are therefore a wasteful use of measurement resources in some stands, and less precise than required in others. To more efficiently estimate the number of sampling units required, a pre-existing knowledge of tolerable error bound for the inventory, and the variability of the resource in question are required. The tolerable error bound can be expressed in absolute terms or as a percentage, in which case it is referred to as the allowable error [10]. The relationship between the sample size (n) required to meet a desired level of allowable error and the coefficient of variation (sample standard deviation / sample mean) is shown in Figure 1. The equation used to calculate sample size is different for a finite and an infinite population. In forestry scenarios, stands are generally considered infinite populations because the sampling fraction employed is below 5% of the total population (N). In Figure 1 the green line shows the relationship between n and coefficient of variation in an infinite population scenario, and the red line shows the relationship for a stand in the study area under a finite population scenario for indicative purposes.
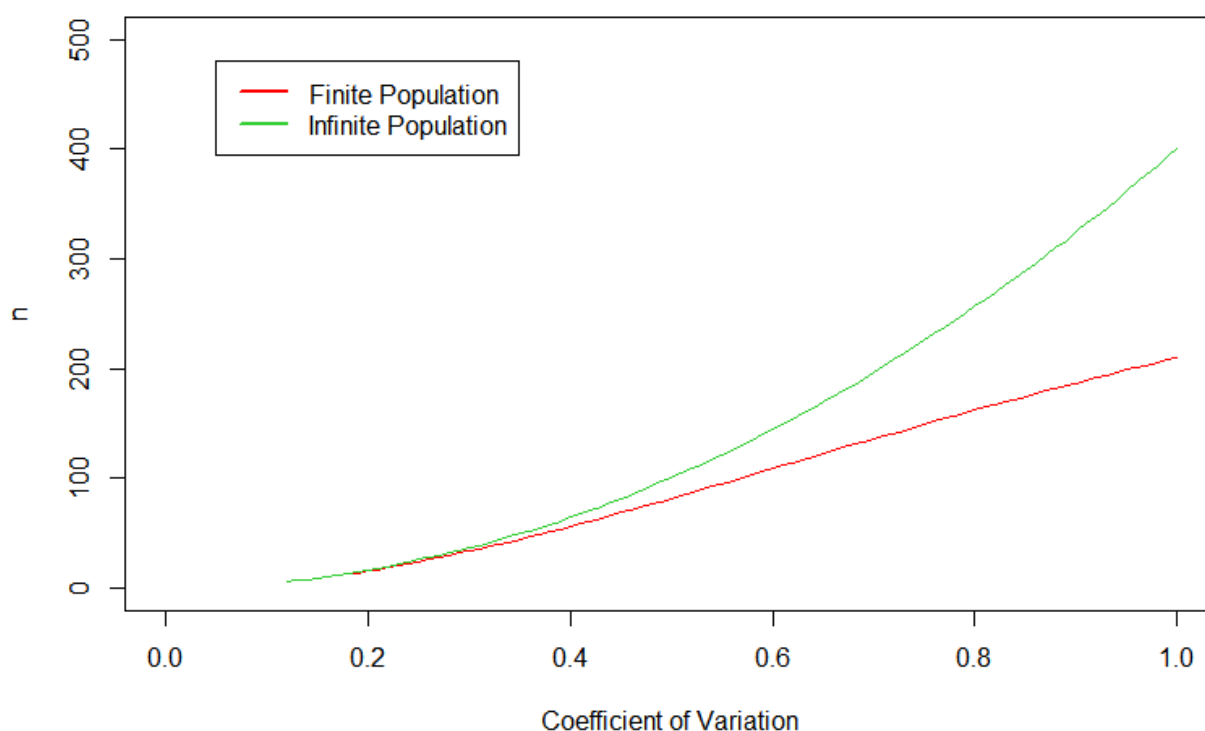

Figure 1. The relationship between sample size and coefficient of variation for an allowable error of 10%

In forest inventory the variance between samples is not known until after the inventory has taken place, and so cannot be used to calculate n. When a resource is large, or valuable enough, a small number of samples or a pilot study may be measured to acquire a measure of the variability in the population that can then be used to calculate a suitable sample size. When remotely sensed data are available during inventory design, this may be used to assess the variation in a population provided it has a strong relationship with the variable of interest.

Numerous studies have shown that aerial LiDAR data have a strong relationship with various forest parameters that are typically measured in forest inventories, including stand volume [13,7], carbon [11], and log product volumes [3]. Given a strong relationship between a LiDAR metric and the variable of interest, the coefficient of variation used to describe the variability in the stand can easily be acquired from the LiDAR point cloud and used to guide sampling design.

A recent study on a national LiDAR dataset in New Zealand (Watt *et al.* 2013) found that the LiDAR metric mean height (H_m) was the most strongly related variable to stand volume, accounting for 83% of the variance of in stand volume using a polynomial form. It may be simplistic to think that models derived at the national level can be applied with confidence to derive stand level estimates. However, assessing the variability in stand volume using the variability in H_m to provide an estimate of the stand variability is a valid approach.

The LiDAR processing software package FUSION [5] was used to calculate LiDAR metrics at a 30-m resolution across the entire forest landscape. Each 30-by-30 m pixel produced contained a value for 101 elevation and intensity metrics which describe the LiDAR point cloud. The variance and mean of the H_m scores for all pixels within a stand boundary were used to calculate the coefficient of variation for each stand. This measure of variance was then used to calculate the sample size required to achieve an allowable error, or PLE, of 10% on total recoverable volume (TRV) using a well-known sample size calculation formula. A forest inventory database was then interrogated to extract the plot numbers and precision estimates for stands in the study area. Only stands greater than 5 hectares were included in the study. The resulting dataset contained 132 stands covering a total area of 2648.8 ha. The actual plot numbers measured and the optimal sample size calculated using the coefficient of variance from H_m are shown in Table 4.

Table 4. Plots measured and optimal sample size (n) and plot costs in the study area

	Plots measured	n finite population	n infinite population
Total	1500	1049	1274
Plots/ha	0.56	0.39	0.48
Cost[1]	$150,000.00	$104,900.00	$127,400.00
Cost/ha	$56.63	$39.60	$48.11

In Figure 2 and Figure 3, each datum represents a stand, and the size of the datum is proportional to the stand's area. The diagonal line has a slope of 1 and an intercept of 0 and reflects a perfect (1:1) correspondence between the number of plots measured and n. Points closer to the y-axis than the diagonal line have more plots installed than the value of n required to achieve a PLE of 10% suggested by the variability in H_m, and the plots closer to the x-axis have fewer. Larger stands are clustered closer to the y-axis indicating that these stands may receive more plots than is necessary to achieve the assessment objective. This is a logical result in a scenario where plot numbers were assigned based on a simple sampling fraction. For a large number of stands the optimal sample size is smaller than expected. This may be because the CV of H_m is smaller than the stand CV in stand TRV. This could be a subject for further research.

---

[1] Cost here is calculated assuming a plot rate of $100 per plot. This is not meant to reflect the actual plot rate.
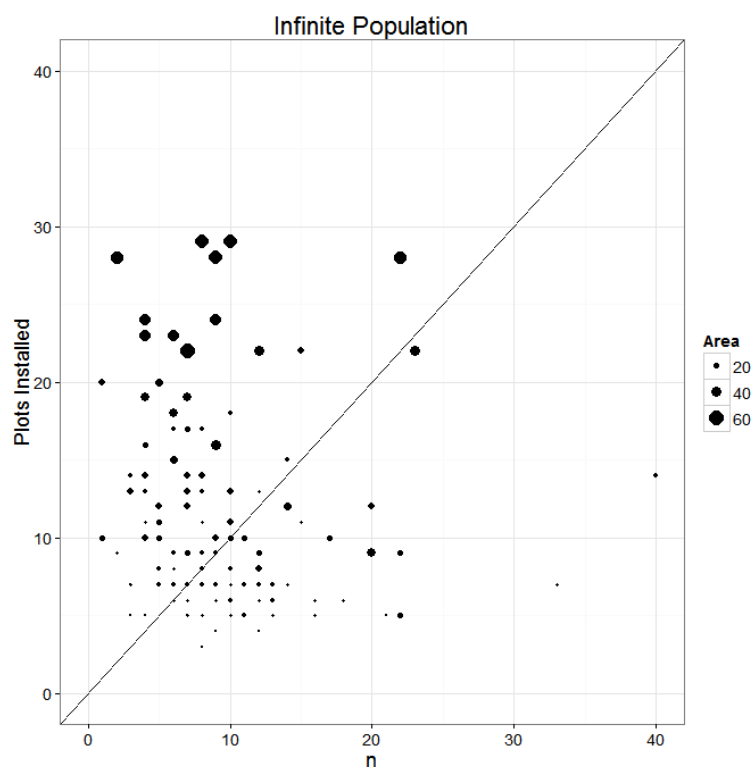
Figure 2: The relationship between n and plots measured in study stands under an infinite population scenario. Stands to the left of the diagonal line can be thought of as having excessive plots measured to achieve a PLE of 10%, stands to the right of the line can be thought of as having too few.
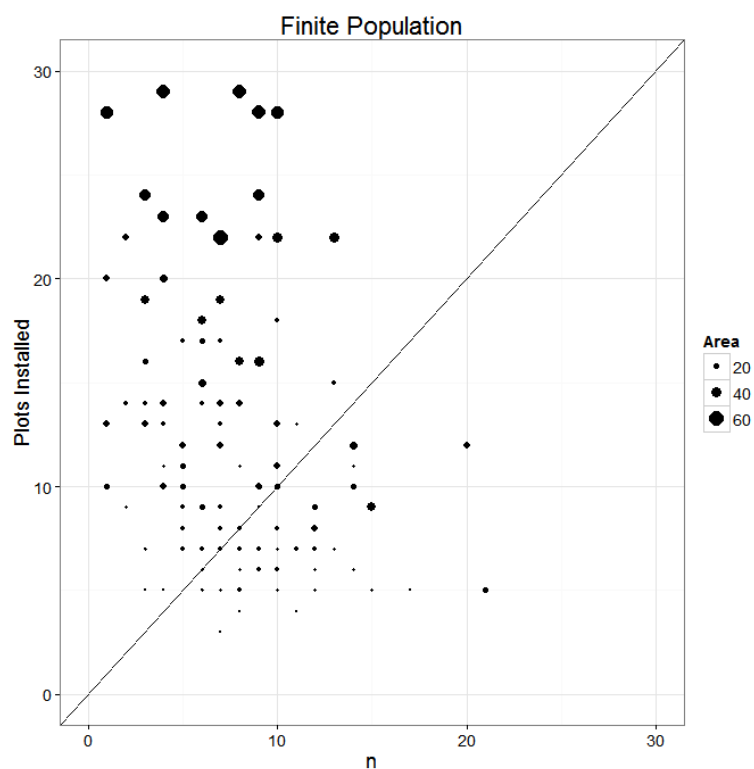

Figure 3: The relationship between n and plots measured in study stands under a finite population scenario. Stands to the left of the diagonal line can be thought of as having excessive plots measured to achieve a PLE of 10%, stands to the right of the line can be thought of as having too few.

The plot and cost savings reported in Table 4 are valid only if the application of n sample plots would provide population estimates with the desired allowable error. Without additional measurement this cannot be known in most cases, but the precision levels and sample size in the installed forest inventories provide some insight. The relationship between the PLE on TRV and the proximity of the actual sample size to n is shown in Figure 4, where each stand in the dataset is represented by a single datum. The solid horizontal and vertical reference lines are placed at a PLE of 10%, the allowable error used in calculation of n, and at 0 (i.e. sample size measured = n) respectively. Stands to the left of the vertical line have fewer plots installed than n and plots to the right of this line contain more. In Figure 4 there is a general trend showing that stands with fewer plots than n tend to have a larger PLE. Stands below the horizontal line have better precision than required by the inventory objectives and those above are too imprecise. Figure 4 shows that generally stands with considerably more plots than n are too precise and stands with considerably less are generally too imprecise to be acceptable under the allowable error objective of the inventory. It should be noted that there is probably a significant component of noise in Figure 4 associated with sampling error.
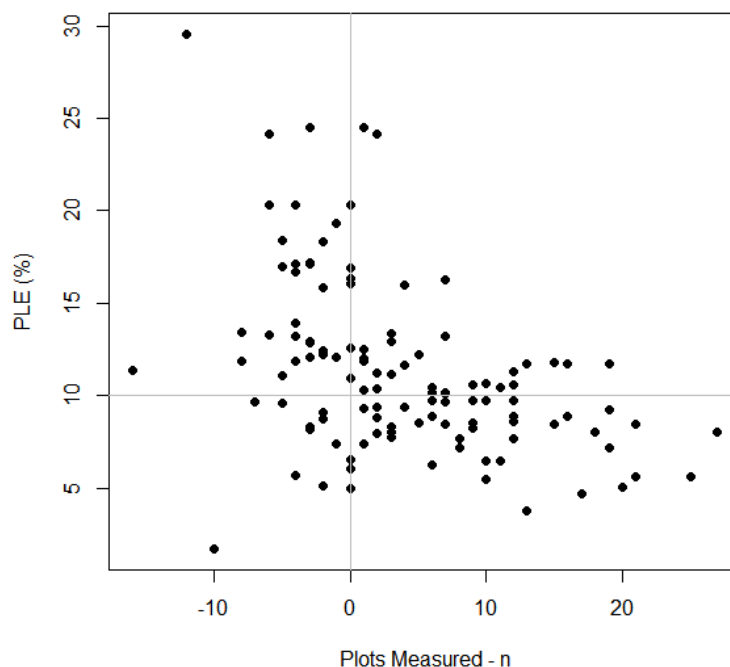

Figure 4: Actual PLE estimated in the subject stand, and the difference between actual sample size and n for infinite population in the study stands.

Excessive precision and excessive imprecision both represent a financial cost to the forest manager. The cost of excessive precision is equal to the additional plotting costs associated with installing more plots than n. In this case, assuming a plot cost of $100, the cost of excessive precision can be deemed to be the difference between the costs of actual plot measurement and the cost of measuring n. The total cost of excessive precision in this scenario, assuming an infinite population, is $22,600.00. The cost per hectare is $8.52[2]. These figures relate specifically to this forest and the measurement scenario reported on herein. Extrapolation of this relationship to other forests in an attempt to quantify savings would be inappropriate and misleading. The cost associated with excessive imprecision is considerably more difficult to quantify and likely to be much larger than that associated with excessive precision.

Using continuous LiDAR data collected over a forest resource in the manner described above is a highly inefficient and limited use of reasonably expensive to acquire remotely sensed data. The

---

[2] The cost of LiDAR acquisition and additional processing may need to be removed from these figures.

information in the LiDAR point cloud provides detailed auxiliary information about each sample point in the population, so estimation techniques other than simple random or stratified sampling should be employed to make use of this. Recent research by Future Forest Research (FFR) has shown that significant benefits can be gained from aerial LiDAR data using regression estimation (Marshall *et al.* 2012) and k nearest neighbour (kNN) estimation [2, 3]. The usability of regression estimation is limited in a New Zealand context because estimates are required at the stand level, and regression estimation requires a minimum sample size per area of interest. By contrast kNN estimation has been shown to be capable of providing accurate and precise estimates for many stands within a forest when LiDAR data are available; even for those stands that contain no ground plots.

The sampling technique known as kNN estimation integrating LiDAR data has now been implemented in three forests, with highly variable terrain types, in New Zealand with encouraging results [3, 2, 4]. Stand dimensions, including log product volumes, were estimated using kNN for all stands in the forest. The sampling error associated with these estimates was also calculated using a technique that accounts for spatial correlation in the field plots [6].In Kaingaroa Forest, stand dimensions were estimated using kNN for a total of 102 stands, and in 229 stands in Tairua. Stand areas in Tairua were considerably smaller on average than in Kaingaroa. The PLE for an area of interest (AOI) is sensitive to the number of donors used for each target pixel (k). Figure 5 shows the median PLE for stands in Kaingaroa and Tairua under three values of k. When k=2, the median PLE in Kaingaroa was 10.09% and 10.96% in Tairua. When k=10, the median PLE in Kaingaroa was 8.47% and 10.16% in Tairua. This result is particularly noteworthy because there were only 99 plots installed in Tairua and 213 in Kaingaroa. Further detail on the inventory outputs in the two forests is given in Table 5.
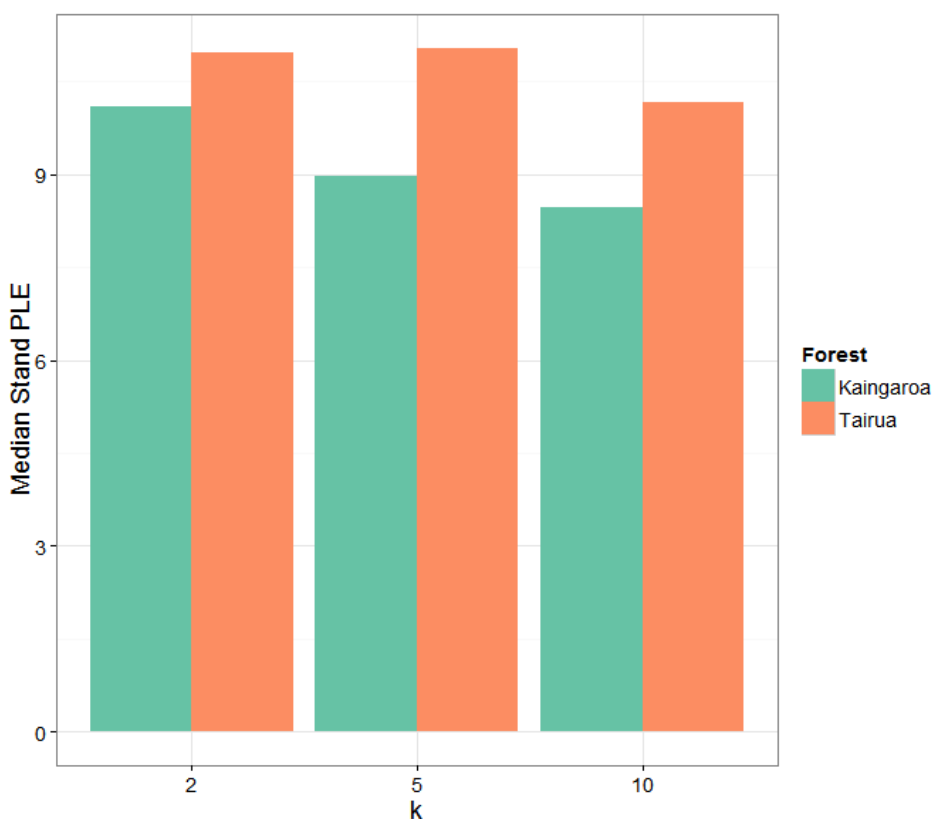

Figure 5. The median stand PLE in Kaingaroa and Tairua calculated for kNN estimates

Table 5: The inventory statistics for Kaingaroa and Tairua

Forest	Estimation Technique	NSA (ha)	Median PLE[3]	Total Cost	Cost/ha[4]
Kaingaroa	kNN	2612.9	8.98%	$42,600.00	$16.30
Kaingaroa	SRS	2202.9	6.2%	$76,200,	$34.59
Tairua	kNN	2683.6	11.03%	$19,800.00	$7.57
Tairua	SRS	2648.8	10.54%	$150,000	$56.63

The magnitude of the cost saving available from using kNN as an alternative inventory estimation technique when aerial LiDAR is available is large and provides a compelling argument for LiDAR acquisition in its own right. Clearly kNN can provide precise estimates of stand dimensions, and the accuracy of estimates when compared to traditional stand assessments has been found to be very high in Kaingaroa [3] and an Eastern Bay of Plenty forest case study [4]. In Tairua [2] there were slightly larger discrepancies between kNN estimates and traditional inventory estimates. There were several reasons for this – notably the sample size (99) used was considerably smaller than that (~200+) recommended for use in kNN estimation [1]. The ground plot sample size in a kNN estimation approach also plays an important part in the size of sampling error. Figure 6 shows the relationship between the distinct count of donors in an AOI and its PLE in Kaingaroa and Tairua. The relationship is not linear but is strongly negative; estimates for AOIs that use many different donors have lower PLEs.
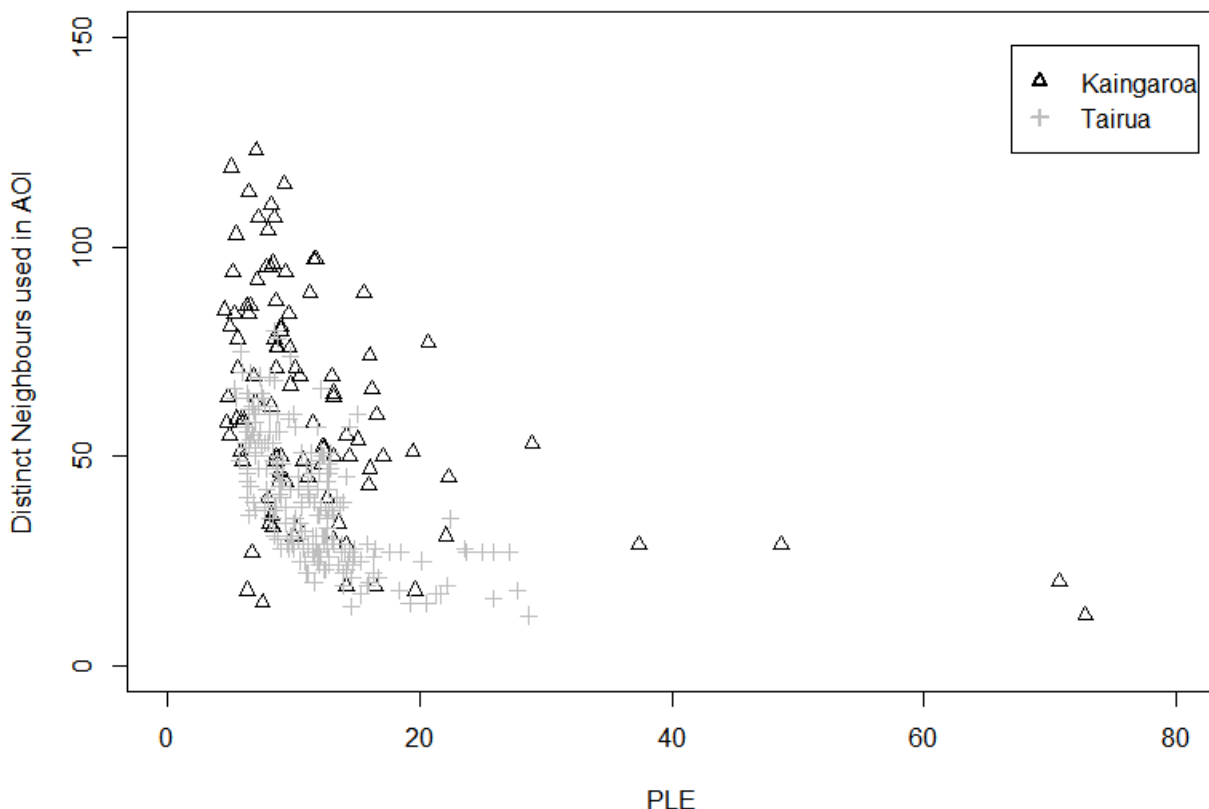

Figure 6: The relationship between distinct neighbours used in an AOI and PLE in two forests.

---

[3] For kNN median PLE estimates k=5
[4] Costs in this table account for the additional processing costs associated with kNN estimation by using a plot price of $200 for kNN estimates and $100 for SRS estimates.

Implications of Results and Conclusions

As a result of the work undertaken to complete Objective 1, the required sample size to meet a specific allowable error objective for any stand where aerial LiDAR data are available can be calculated. The cost implications of sub-optimality have also been examined. Furthermore an alternative inventory estimation technique that makes better use of the remotely sensed LiDAR data has been implemented and the cost implications of this approach have been examined. These results show that significant savings in plot numbers, and associated costs, can be made by following the kNN estimation approach. The cost savings reported here are specific to the forests under study and cannot necessarily be extended to other forests. However this work further supports the use of kNN estimation as a valuable inventory estimation technique where aerial LiDAR is available.

Objective 2

Use LiDAR data to develop maps describing site index and age of final thinning

Methodology and Results

This section addresses Objective 2 of the Tairua case study work plan; this objective aims to use aerial LiDAR data to produce maps of site index and target thinning age for Tairua. There are a number of approaches available to calculate site index from LiDAR data that include modelling mean top height from the LiDAR data and using stand records for stand age. The P_{99} metric is known to be extremely highly correlated with mean top height (MTH), and numerous studies have used this metric as a surrogate for various measures of stand height. For the reference dataset in Tairua, the 99th height percentile in the LiDAR (P_{99}) was found to be the most highly correlated (R=0.96) metric with MTH. A linear regression model was fitted between MTH and P_{99}, and was found to explain 90% of the variation in MTH ($R^2 = 0.90$, p<0.001). The model developed had a slope of 0.91 and an intercept of 3.78 with all terms significant at the 95% significance level. Figure 7 shows the relationship between MTH and P_{99} for the plots in the reference population in Tairua.
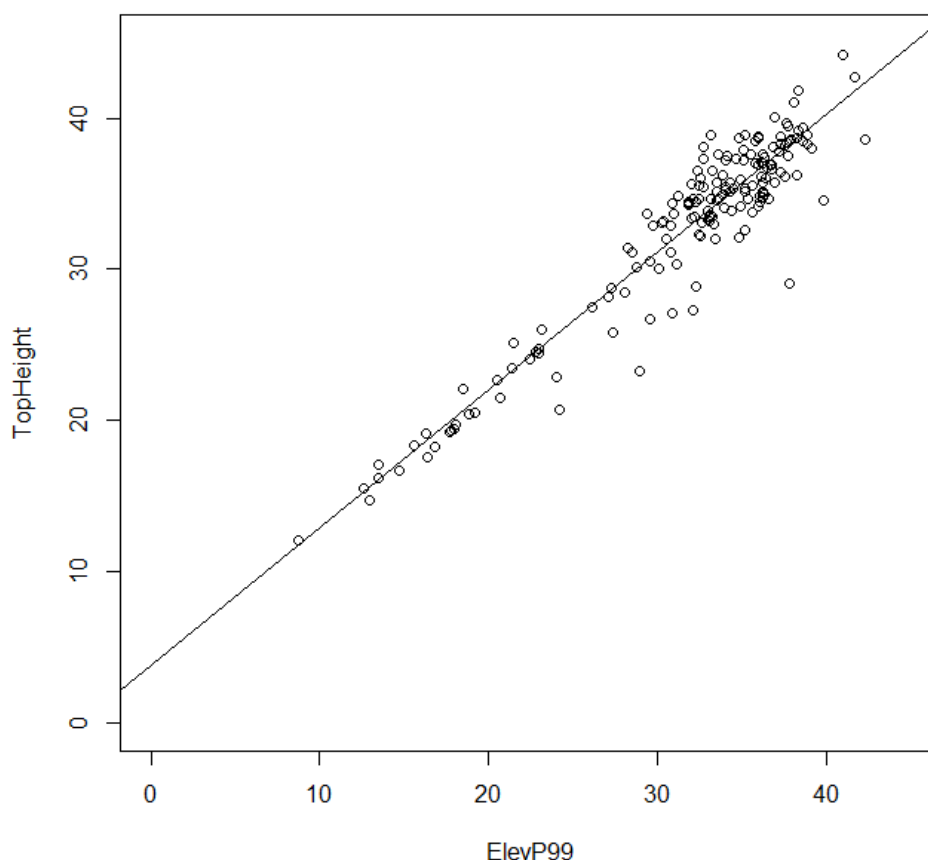

Figure 7. Mean top height and P_{99} in Tairua

Using this model, MTH was calculated for each pixel in the target dataset based on P_{99} and age extracted from the forest manager's stand records. This calculated MTH was then used in the calculation of site index. In New Zealand for radiata pine, site index is typically defined as MTH at a reference age of 20. There are many methods for the calculation of site index, but it is regularly calculated through an inversion of height-age models [12] and there is a wide variety of model forms available. The site index model associated with the 300 Index growth model as implemented in the forest simulator FORECASTER is as close to an industry standard methodology as exists in New Zealand, and was selected for use in this study. The FORECASTER site index is calculated by solving for zero using bisection by the following equation:

HMTH - CalcMTH(x,HAge)

    Where x = SI

          HAge = Measurement age

        HMTH = Modelled MTH

        CalcMTH = 0.25 + (SI - 0.25) * ((1 - Exp(-ha * HAge)) / (1 - Exp(-ha * 20))) ^ hb

        Where ha = hae1 + hae2 * latitude + hae3 * elevation

            hb = 1 / (hbe1 + hbe2 * SI)

          Where   hae1 = 0.1409

                hae2 = -0.00196

                hae3 = -0.0000338

                hbe = 0.5141

                hbe2 = 0.00457

Elevation was derived from a digital terrain model produced from the ground classified points in the LiDAR point cloud over Tairua. A 30-m pixel resolution was used to describe elevation. A latitude of 37 degrees was assumed for the forest, as fine resolution variation in latitude has little effect on site index. Using this method, site index was calculated for each 30-m pixel across the study area, resulting in a detailed site index surface. Table 6 summarises the inputs into the site index calculation, and the surface is displayed in Figure 8.

Table 6: The range of input values used to calculate site index

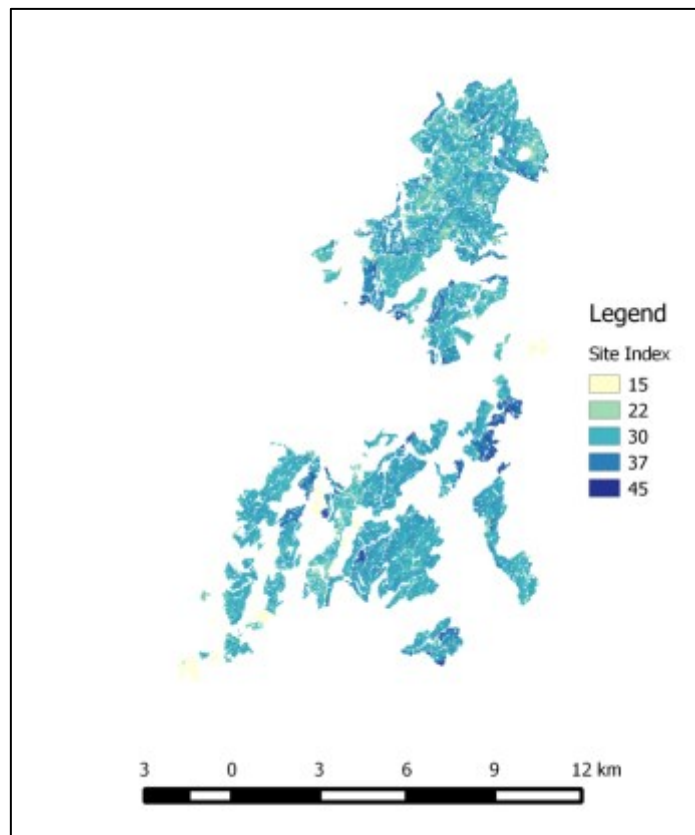|	MTH (m)	Stand Age (y)	Elevation (m)	Latitude
Mean	20.89	14.01	118.63	37
Range	4.27 – 68.22	5 - 52	532.11 - 1	

Figure 8: Site index map derived for Tairua based on the LiDAR dataset.

Two pre-existing site index surfaces that cover the study forest were compared to the surface produced from the LiDAR dataset. The pre-existing site index surfaces had a resolution of 25 m [8] and 1000 m [13] respectively. To provide a comparison with the pre-existing site index model, the predicted site index for all stands in Tairua were calculated by aggregating the pixels within the forest manager's stand boundaries. This information is summarised in Table 7, and Figure 9 displays difference maps for the site index calculated from the LiDAR dataset and the two pre-existing site index surfaces. Table 7 shows that on average the site index values calculated from the three surfaces are similar. This is despite the fact that the LiDAR-derived site index surface and that produced by Palmer *et al.* [8] are at a much finer resolution than that produced by Watt *et al.*[13]. The site index difference maps below show that there is greater agreement between the LiDAR-derived index surface and Palmer *et al.* [8] than with Watt *et al.* [13] but the agreement at the stand level indicates that the resolution of the surfaces is a major contributor to this. This work shows that an accurate site index surface can be calculated without any field measurements. The result here also serves to validate the accuracy of the pre-existing national surfaces of site index for this forest.

Table 7. Summary of site index values for stands in Tairua

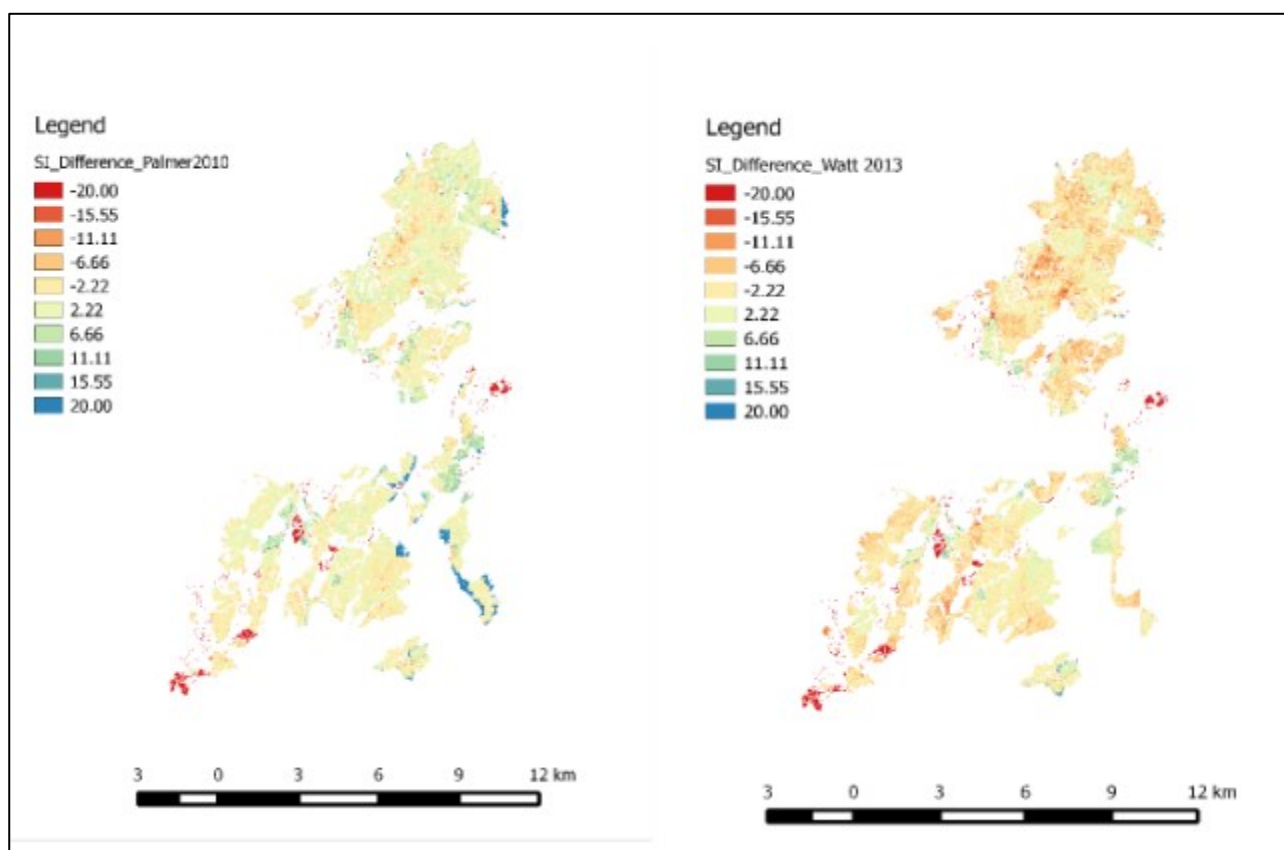| SI Surface	Current study	(Palmer *et al.* 2009)	(Watt et al.2013)
Mean Stand SI	30.87m	30.14m	31.71m
Stand Dev SI	4.01m	2.84	7.3
Min SI	16.93	1.28	0
Max SI	49.32	33.94	37.74

Figure 9: Site index difference maps for Tairua.

A further element of Objective 2 was to calculate the age of final thinning based on the LiDAR data under the assumption that final thinning occurs at a target stand height of 15 m. Using the site index values calculated by pixel in the forest it is possible to calculate the age of thinning through bisection by solving for zero the following equation:

CalcMTH (SI, Age) - 15
       Where SI = calculated site index based on LiDAR
           HAge = Measurement age
         HMTH = Modelled MTH
         CalcMTH = 0.25 + (SI - 0.25) * ((1 - Exp(-ha * HAge)) / (1 - Exp(-ha * 20))) ^ hb
         Where ha = hae1 + hae2 * latitude + hae3 * elevation
              hb = 1 / (hbe1 + hbe2 * SI)
           Where   hae1 = 0.1409
                       hae2 = -0.00196
                       hae3 = -0.0000338
                       hbe = 0.5141
                       hbe2 = 0.00457

Using this approach, the distribution of the target thinning age was mapped across Tairua (Figure 10). Describing the distribution of target thinning age between and within stands can now easily be achieved by loading the target thinning age surface into a GIS. Aggregation and averaging of pixels within a stand boundary will provide an estimate of target thinning age for a stand that can be used for planning operations.
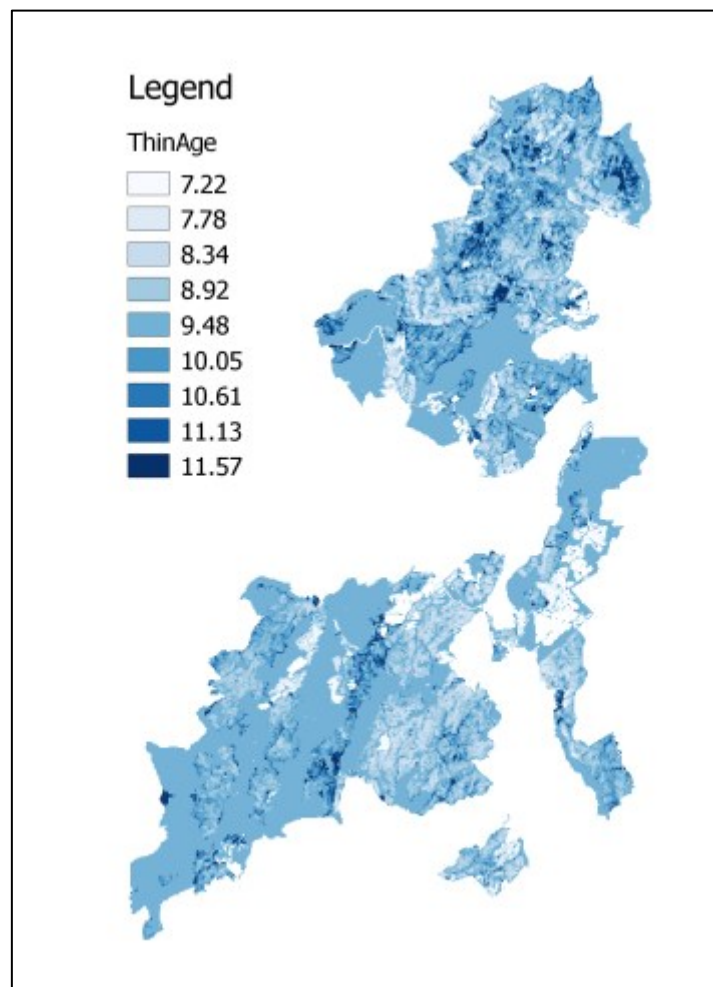

Figure 10: The target final thin age for Tairua derived from the LiDAR data.

Implications of Results and Conclusions

The work undertaken to complete this objective means that site index can be calculated for any patch of forest that has aerial LiDAR data where the planting year is known. Maps detailing the distribution of site index within and between stands have been produced. The close correspondence between the stand level site index values derived from LiDAR and the pre-existing national site index surfaces reflects positively on the validity of all three models.

Objective 3

Evaluate whether LiDAR data can be used to accurately derive estimates of 300 Index.

Methodology and Results

Objective 3 of the current case study is to evaluate whether LiDAR data can be used to accurately derive estimates of 300 Index. The 300 Index is an alternative measure of site productivity that specifically refers to the mean annual increment (mai) of a stand at age 30 grown under a standard clear wood regime thinned to a density of approximately 300 stems per hectare (sph) prior to harvest at age 30. The 300 Index for a given patch of forest can be estimated using bisection, in a manner similar to the estimation of site index above, by solving for zero using the equation

<p style="text-align:center;">Measured dbh – final dbh at harvest age</p>

Solving this for each pixel in the forest in the same manner as for site index in Objective 2 is possible but would require the implementation of the 300 Index growth model into a programming language, and this has a high degree of complexity. Furthermore the volume and stocking for every pixel would need to be modelled from the LiDAR data. Again this is possible but there would likely be a high degree of error associated with these estimates, and the magnitude of this error would be difficult to quantify.

An alternative, and more efficient, approach is to bypass the modelling of the intermediary steps such as pixel level stocking and volumes, and instead to impute the 300 Index directly from the modelled plots. To achieve this, the 300 Index at measurement date for all ground plots in the reference population was calculated using the implementation of the 300 Index growth model embedded in the yield analysis software package YTGEN [9]. Using the kNN estimation technique, the distribution of 300 Index within and between stands in Tairua could be modelled. Figure 11 shows the distribution of 300 Index across the forest and Table 8 shows a summary of the stand level 300 Index values, with comparison to surfaces derived previously from environmental variables.
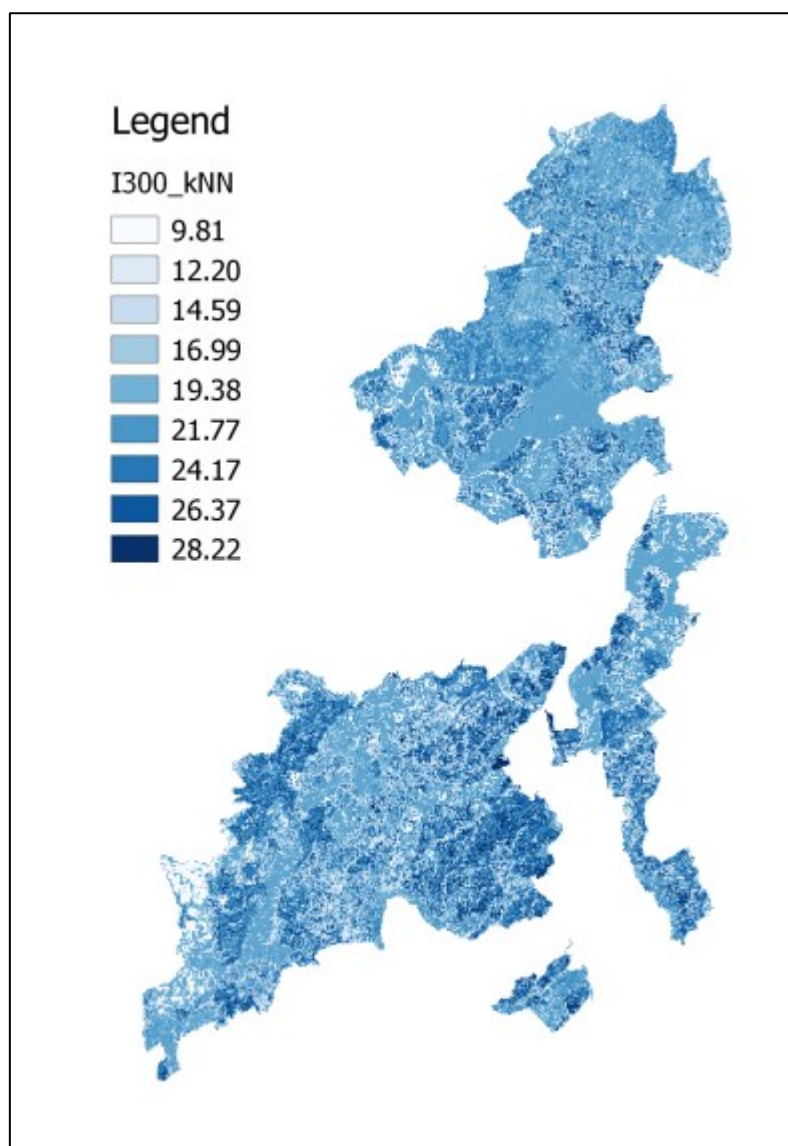
Figure 11: A 300 Index surface (k=2) derived from the LiDAR data and ground plots.

Table 8: A summary of the stand level 300 Index values.

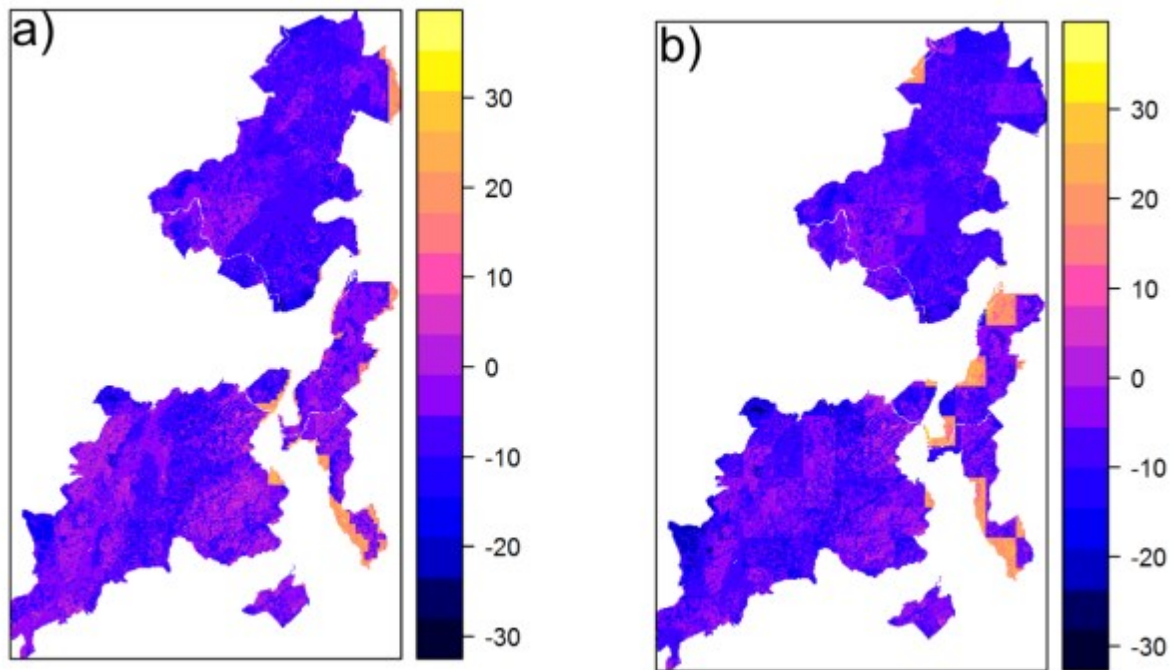| I300 Surface	Current study	(Palmer *et al.* 2009)	(Watt *et al.*2013)
Mean Stand I300	22.23	25.69	25.96
Stand Dev I300	2.30	4.16	6.38
Min I300	9.81	0.97	0.01
Max I300	30.79	33.31	34.93

Figure 12: The difference between the 300 Index values predicted from LiDAR metrics and those from Watt 2010 (a) and Palmer 2009 (b).

Implications of Results and Conclusions

As a result of this work a methodology has been developed for describing the distribution of the 300 Index within and between stands based on LiDAR data and a small number of ground plots.

Objective 4

Validate the accuracy of tree counting using both ground and image calibration methods.

Methods

In the interest of limiting field work, some larger stands were sub-sampled by manually removing polygons from the whole stand shapefile. All stands were assessed with tally plots on a grid with random origin and orientation. Refer to Table 3 for the details of the stands sampled and plot sizes used. Tree count (tally) and a visibility score for each tree crown were made in each tally plot. Tally plots were sized to contain 20 trees, using stocking recorded in the stand records. Two tally plots were randomly selected in each stand for measurement of DBH on all trees, and STAV (standing tree acoustic velocity) on a maximum of 15 trees per plot. For the M age class, DBH was measured in all tally plots.

Stands S1, S3, S5, M1, M3, M5, P1, and P3 were evaluated for tree count accuracy using the VPlot methodology. Stand P5 was excluded as it contained only two tally plots, insufficient for processing.

The LiDAR was processed to produce a CHM (Canopy Height Model) image for each stand with 0.25 m pixel size. Calibration counts from the ground plot tallies, plot visibility counts and plot counts on images by two operators were used to evaluate three count methods referred to as the Ground, Visible and Image methods respectively.

Bias, standard error and root mean squared error, expressed as percentages, were used as measures of counting error. Bias was estimated for the Image method only, as the average of plot level differences between the operator image counts and ground counts for the plots.

Key Results

Initial review of results showed ground counts for stand S1 were almost double the counts on the image by both operators. Investigation showed this stand had heavy regeneration which the ground crew had difficulty distinguishing from the crop trees. As a result this stand was excluded from count tests, as a reliable reference count could not be determined.

Table 10 presents mean bias, standard error (SE) and root mean squared error (RMSE) for the Reference, Ground, Visible and Image count. Figure 12 presents RMSE for the four methods. The reference count has an RMSE of almost 7%, while that observed at Kaingaroa (K) was 6%. The Ground and Visible methods are effectively equal with the lowest error, RMSE just under 6% (K 5%). Image method has overall negative bias of just over 7% and RMSE of just under 11% (K 11%). SE for the Image method is half that of the ground-based methods.

Table 10: Error by count method.

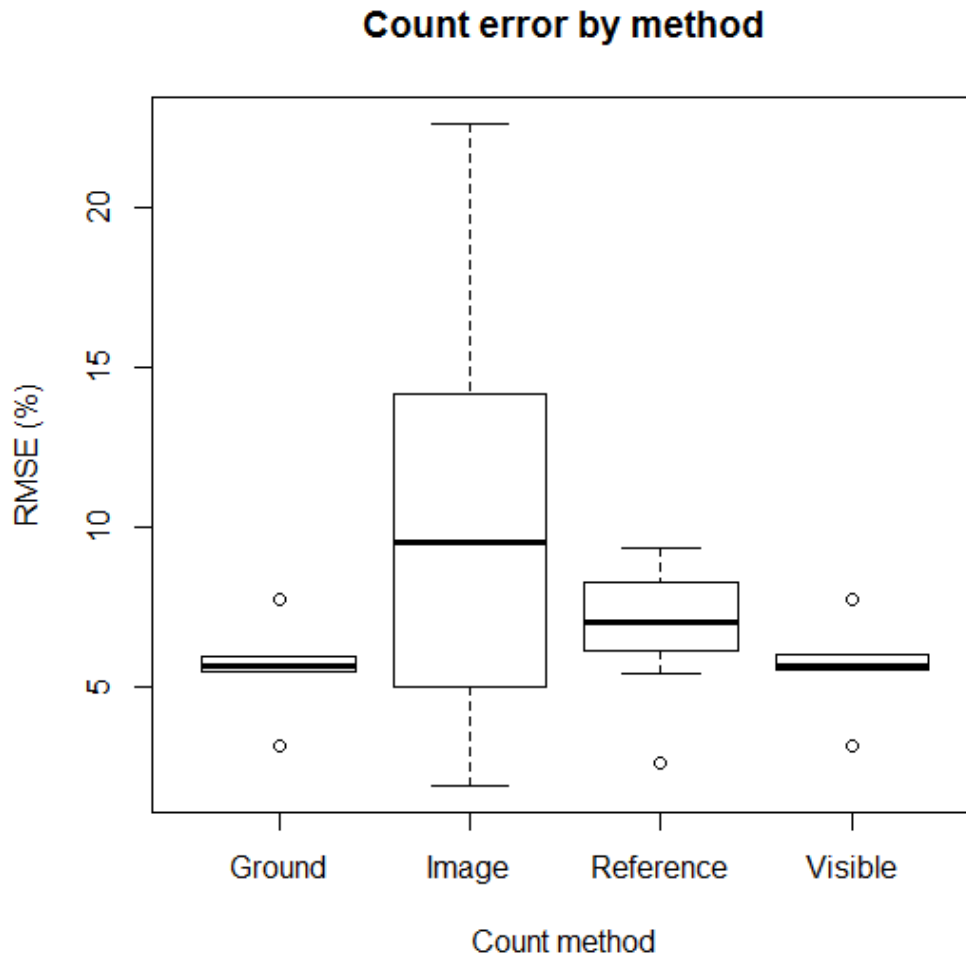| Count method	Bias (%)	Standard error (%)	Root mean squared error (%)	Number of tests
Reference	0.00	6.81	6.81	7
Ground	0.00	5.60	5.60	14
Visible	0.00	5.64	5.64	14
Image	-7.35	3.13	10.81	14

Count error by method

Figure 12: Root mean squared error (percentage) by count method.

Table 10 gives individual count results for each stand and operator (n=1) for the Image method. Inspection of those results showed errors for operators tended to agree for each stand.

Table 10: Error by operator and stand for the Image method.

Operator	Stand	Bias (%)	Standard error (%)	Root mean squared error (%)
O1	M1	-8.43	4.36	9.49
O2	M1	-22.29	3.82	22.61
O1	M3	-13.93	2.69	14.18
O2	M3	-22.48	2.31	22.60
O1	M5	-9.27	2.40	9.58
O2	M5	-7.74	2.43	8.11
O1	P1	9.56	7.45	12.12
O2	P1	7.80	1.99	8.04
O1	P3	-1.67	4.08	4.41
O2	P3	-4.27	2.57	4.99
O1	S3	0.00	2.21	2.21
O2	S3	0.31	1.89	1.92
O1	S5	-17.67	2.74	17.88
O2	S5	-12.88	2.90	13.20

In Table 11 average count results are given by stand, ordered by age. No trends were observed in error measures for the Image method by age class or stand age.

Table 11: RMSE by stand, ordered by age, for the Image method.

Stand	Age	Bias (%)	Standard error(%)	Root mean squared error(%)
S3	12.56	0.15	2.05	2.06
S5	13.54	-15.27	2.82	15.54
M5	20.56	-8.50	2.41	8.84
M1	20.56	-15.36	4.09	16.05
M3	21.56	-18.20	2.50	18.39
P3	24.56	-2.97	3.33	4.70
P1	25.58	8.68	4.72	10.08

Table 12 presents average error by operator using the image method. Overall there were no obvious differences between the two operators.

Table 12: Error by operator for the Image method.

Operator	Bias (%)	Standard error (%)	Root mean squared error (%)	Number of tests
O1	-5.92	3.70	9.98	7
O2	-8.79	2.56	11.64	7

Implications of Results and Conclusions

The results generally re-confirm those found at Kaingaroa. Count methods using ground calibration deliver 6% RMSE, and image-based calibration results in RMSE of 11%. The ground calibration method delivers an improvement of 1.2% in RMSE over use of ground plots alone. There was no overall difference between operators with the Image count method.

There was no significant improvement in RMSE from recording visibility scores for tree crowns, indicating the extra effort is not warranted. A number of stands had significant regeneration, but this seemed to be as likely to introduce error into the ground count as the estimated counts from tree detection. Stand S1 was excluded from count tests as it was badly affected by confusion between crop and regeneration trees in the reference ground counts. In this situation the image-based count would possibly give a more accurate estimate of the crop tree count than the ground count.

The Image count method had an overall negative bias, unlike Kaingaroa where bias was over and under. There was no trend in RMSE for the Image method by stand age or age class. Inspection of images for stands with the lowest RMSE showed they had more regular crown size, shape and spacing. The low SE of the Image method is notable, and was also observed at Kaingaroa. This is attributed to the fact that with the Image method, both operator and algorithm count on the image, so there is good agreement in plot level counts. With ground calibration (Ground and Visible methods), ground plot counts are compared with image counts from the algorithm. GPS error in plot locations and tree tops that lean in or out of the plots results in differences between ground and image plot counts, giving rise to the higher SE observed with the ground calibration methods. The observed increase in SE attributed to these effects is just 2.5%.

The accuracy results are a good validation of the VPlot methods given the more complex topography, stand boundaries and stand structure at Tairua and the lower resolution of the LiDAR than at Kaingaroa (specified two and four pulses per metre respectively). Improvement in RMSE obtained by ITD over and above that from ground plots alone may be sufficient to warrant use of ground calibration where lower error is required. The higher error of the image count method may be acceptable for some management applications, and has the benefit of not requiring ground plots.

Further refinement of the Image count method by reducing bias is seen as desirable for research and operational uses of ITD. This will most likely be achieved by focussing effort into creation of better imagery to assist operator interpretation, and development of training and quality checking procedures to improve operator interpretation skill and repeatability

Objective 5

For MRI establish if a stem list can be derived from LiDAR that allows generation of a yield table.

Methods

Plot averages were derived from individual tree DBH and height measurements for the set of 97 MG plots. Two plots (67 and 83) of the original 99 that were extreme outliers were excluded. Individual tree detection (ITD) was carried out on the MG plots, and plot averages were calculated from the set of 50 crown metrics that were derived for each tree. The ground and crown metric plot averaged data were then used to develop models of diameter and height based on crown metrics. The models were then used to estimate DBH and height for every tree detected in a set of MRI stands. Stand DBH distributions from the model were compared with those from plot measurements.

Key Results

Figure 13 shows the wide ranges of plot means for DBH and heights measured in the kNN plots.
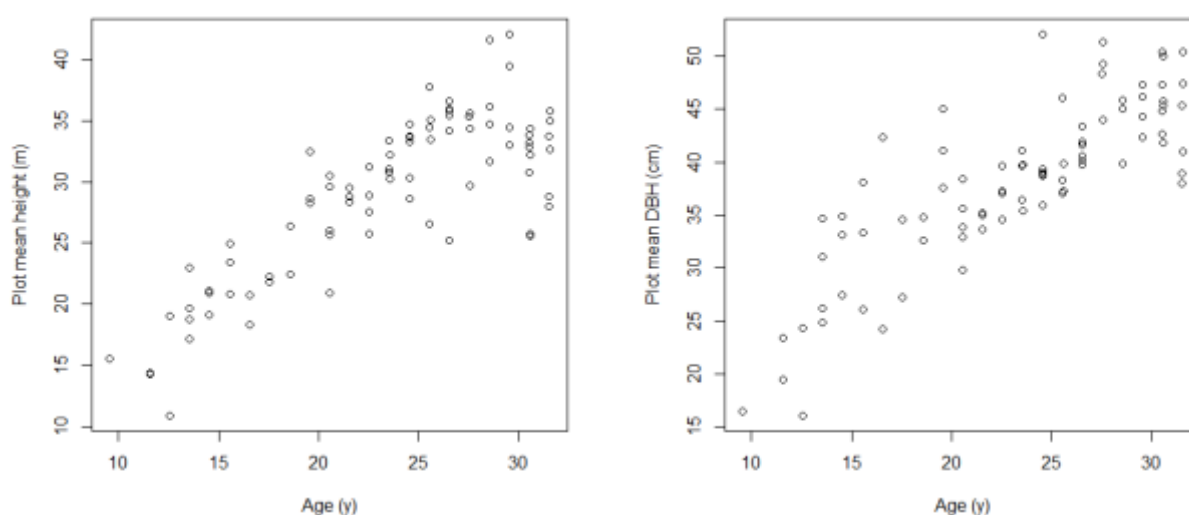

Figure 13: Plot means for DBH (left) and height (right) measured in 99 kNN plots, plotted against stand age.

Correlations were examined to determine the best crown metrics for use in models. For mean tree height, the best crown metric was CHMHeight, with a Pearson's correlation coefficient of 0.96. For mean DBH the best crown metric was CrownFullVolume, with a Pearson's correlation coefficient of 0.88.

A linear model fitted to estimate tree height is given in Equation 1. Analysis revealed no useful additional predictor variables and no trends in the residuals for the model, which had an R-squared of 0.93 and RMSE of 1.75 (6.0%).

$$H = 0.90012C + 5.26305 \qquad\qquad\qquad \text{Equation 1.}$$
where:

      H is plot mean height

      C is CHMHeight

The relationship between CrownFullVolume and DBH was non-linear, and a Gompertz function was fitted (Equation 2). The fit index, analogous to R^2, of the model was 0.83, an improvement over 0.78 obtained with a linear model. RMSE of the DBH model was 3.9 (8.3%). Further analysis revealed no useful additional predictor variables, and no trends were observed in the residuals.

$$D = a_0 \exp(-b_0 b_1^x) \qquad \text{Equation 2.}$$

where:

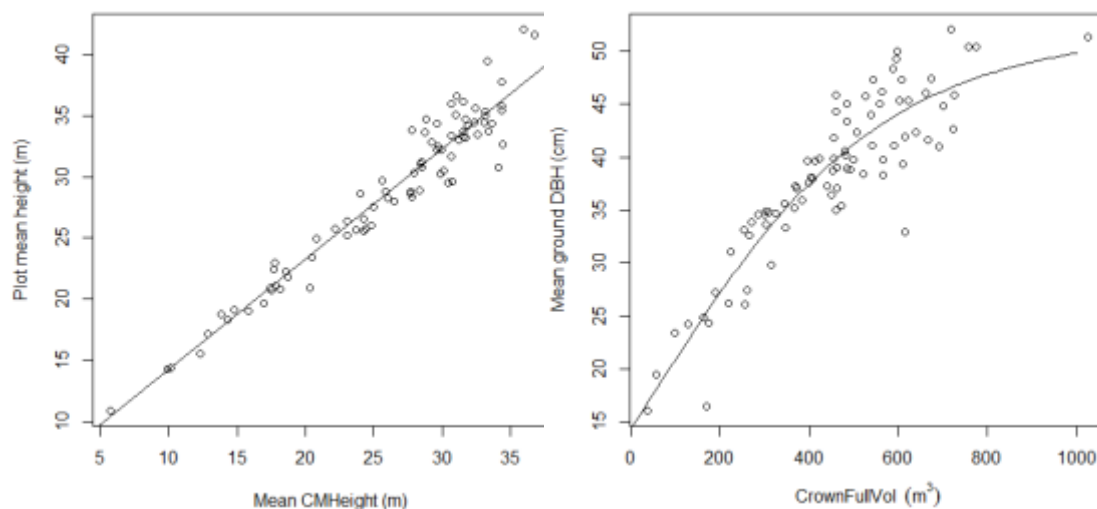|	
a_0	is 51.9231706
b_0	is 1.2818118
b_1	is 0.9965808
x	is CrownFullVolume

Figure 14: Fitted models and data points for height (left) and DBH (right).

The input data and fitted models for height and diameter are shown in Figure 14. It is interesting to note the similarity of the ITD-based height data to the area-based LiDAR height data presented in Figure 7. The model for height (Fig. 14, left) appears to give a good fit to the data, with increased error likely for heights above 30 m. The non-linear model for DBH (Fig. 14, right) appears to give an acceptable fit to the data, with higher errors expected for DBH above 40 cm. Higher variation at higher values evident for both models is a sign of heteroscedasticity which may require more sophisticated modelling approaches in the future, but the models are judged sufficiently robust for this investigation.

The models for height and DBH were applied to five MRI stands to estimate a DBH and height for every tree detected by the ITD methods. DBH was measured in bounded plots established in the five MRI stands. Figure 15 represents the cumulative distributions of measured and estimated DBH for the five stands. In all cases the estimated distributions have noticeably more trees in the lower and higher DBH classes than the measured distributions. The estimated distributions also appear truncated at the upper end.
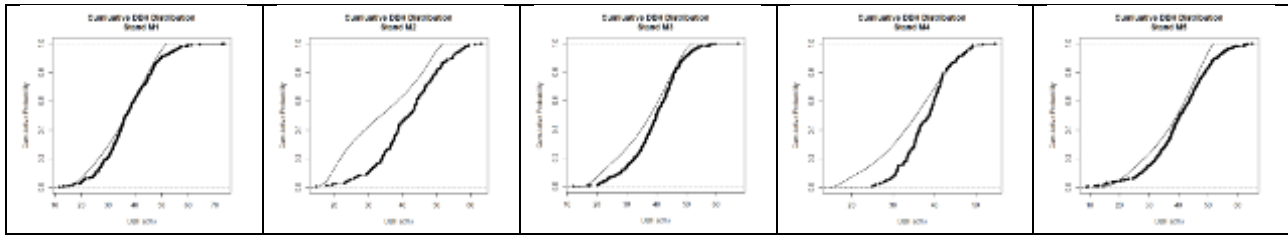
Figure 15: Cumulative distributions for measured (black points) and estimated DBH (line) for five MRI stands.

Table 13 includes *p* values from Kolmogorov-Smirnov (KS) tests applied to compare measured and estimated DBH distributions for the five MRI stands. The *p* values represent the probability the two distributions were sampled from the same population. The low *p* values observed for all five stands indicate that the measured and estimated DBH distributions are significantly different. The *p* values in Table 13 also reflect the degree of difference. Comparing *p* values and plots in Figure 15, we can see measured and estimated distributions are closest for stand M1, and the greatest difference occurs with stand M2.

Table 13: Results of DBH estimation for five MRI stands.

Stand	Number of plots	Number of measured trees	Number of estimated trees	KS p *value*
M1	36	333	12270	0.007927
M2	9	165	4849	1.998E-15
M3	23	450	22142	2.085E-08
M4	11	158	12866	1.022E-07
M5	42	438	8641	3.527E-06

The estimated height distributions for the five MRI stands are shown in Figure 16. Tree heights were not measured in the plots where DBH was measured, and as a result it was not possible to validate estimated heights for these stands. The estimated distributions appeared reasonable, all having a similar normal-curve shape with a slight skew to the right.
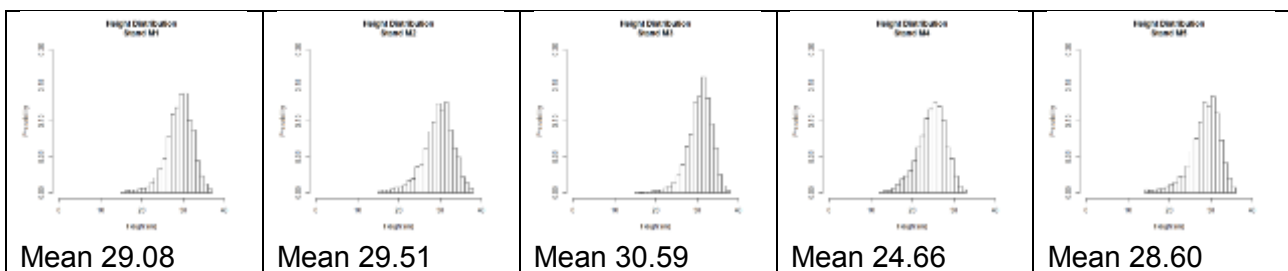

| Mean 29.08 | Mean 29.51 | Mean 30.59 | Mean 24.66 | Mean 28.60 |

Figure 16: Probability distributions of estimated height for five MRI stands.

Detection of single trees across the whole population using ITD methods might provide a more detailed description of the population, and hence a better estimation of yield. Input to yield estimation software is often in the form of DBH and height measurements from bounded (and perhaps angle gauge) plots. Typical inventory practice is to measure DBH of every tree, and heights on a subset covering the diameter range. A height diameter relationship is fitted and used to estimate heights for trees not measured. Such inventory data can be used to provide a tree list which includes a DBH, height and weight for every tree, the latter meaning the number of trees per hectare represented. ITD methods allow the possibility of producing a tree list that includes every detected tree by applying models to estimate DBH and height. This would give the most detailed representation of the stand in terms of DBH and height, but might have excessive data processing or storage requirements in yield estimation software.

Estimated DBH and height distributions and a plot of estimated height against estimated DBH for all 8641 trees detected in stand M5 are shown in Figure 17.
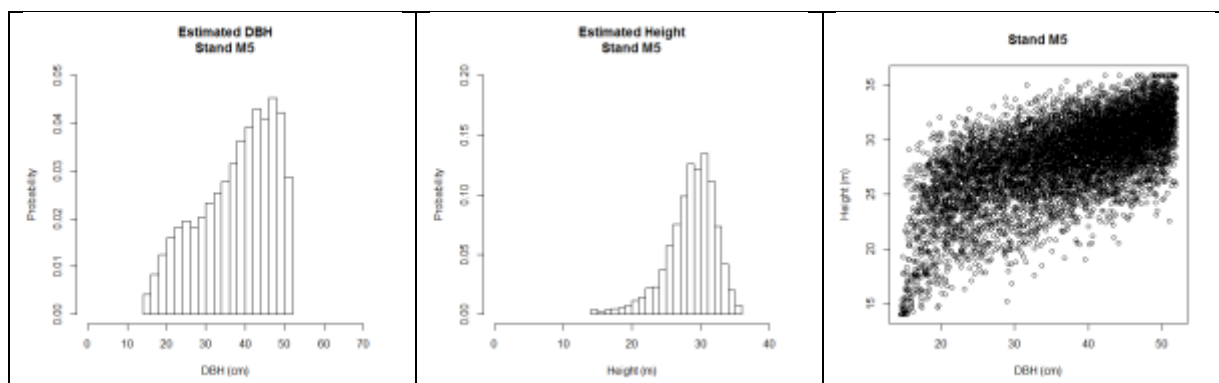

Figure 17: Estimated DBH and height for stand M5, distributions for DBH and Height and height plotted against DBH for all 8641 trees detected.

Tree lists representing every tree would range in length from almost 5,000 to over 20,000 trees for the five MRI stands in this study. To reduce the length of a tree list, the observed ranges for DBH and height can be divided into a chosen number of even classes, as they are in the histograms in Figure 17. For example both the DBH and height ranges could be divided into 20 equal width classes, giving a total of 400 possible DBH / height pair classes. The number of trees observed in each class would be used to determine the weight for the tree list. Some DBH / height combinations would not be observed resulting in a tree list with less than the 400 possible items. This approach would allow the length of the tree list to be easily controlled, balancing processing requirements with degree of detail. Reducing list length by classifying DBH and height does not adapt well to inventory where trees are cruised. The best use of measured data in combination with ITD in that case might be use of imputation methods, applied at the tree level rather than the plot / patch level.

Implications of results and conclusions

Estimation of tree height from crown metrics appeared to give reasonable results. LiDAR is known to give a useful measure of total height at the patch level, and this probably extends to the tree level, albeit with more noise, dependent on point density. This observation is backed up by comparing Figures 7 and 14, showing a strong relationship between height and ITD-based height metrics (Fig. 14), which show slightly more variation than the relationship based on area-based LiDAR metrics (Fig. 7).

Although a model to estimate DBH had a reasonably good R-squared of 0.8 the diameter distributions generated by applying the model did not closely match those observed in ground measurements. More specifically, the model appeared to over-estimate the numbers of trees at the low and high ends of the DBH distribution. A better model may be required, addressing issues of non-linearity and heteroscedasticity observed during analysis. Errors in estimating DBH are also likely to stem from errors in the crown identification and delineation processes.

The data used in this study did not include individual tree locations which required tree level ground measurements and tree level crown metrics to be averaged to plot level for analysis. This potentially weakened observed relationships between ground and crown measures. Error in GPS plot locations also weakens observed relationships, as the plot averages from ground and crown measures can be of a slightly different set of trees.

Future work should attempt to solve the problem of accurately locating individual trees, alone or within plots. Better spatial correlation of single tree ground and crown measures will allow more meaningful evaluation of crown metrics for estimation of individual tree attributes, including generation of tree lists. Accurate location of single trees would permit closer investigation of derived crown metrics and permit further development of the individual tree detection and delineation methods.

ACKNOWLEDGEMENTS

REFERENCES

Breidenbach, J., Nothdurft, A., & Kändler, G. (2010). Comparison of nearest neighbour approaches for small area estimation of tree species-specific forest inventory attributes in central Europe using airborne laser scanner data. *European Journal of Forest Research, 129*(5), 833-846.

Dash, J. P., Marshall, H. M., & Rawley, B. (2013a). Extension Nearest Neighbour Imputation of Stand Attributes using LiDAR data- Additional Dataset: Tairua Forest. Future Forest Research.

Dash, J. P., Marshall, H. M., & Rawley, B. (2013b). FFR Technical Report - kNN Imputation of Stand Attributes using LiDAR. Unpublished: Future Forest Research Limited.

Marshall, H. M., & Dash, J. P. (2013). FFR TEchnical Note: The effect of sample size kNN stand estimates in an Eastern Bay of Plenty Forest. Unpublished: Future Forest Research Limited.

McGaughey, R. J. (2013). FUSION/LDV: Software for LiDAR Data Analysis and Visualisation. (3.30 ed.): United States Department of Agriculture.

McRoberts, R. E., Tomppo, E. O., Finley, A. O., & Heikkinen, J. (2007). Estimating areal means and variances of forest attributes using the k-Nearest Neighbors technique and satellite imagery. *Remote Sensing of Environment, 111*(4), 466-480.

Næsset, E. (1997). Estimating timber volume of forest stands using airborne laser scanner data. *Remote Sensing of Environment, 61*(2), 246-253.

Palmer, D. J., Höck, B. K., Kimberley, M. O., Watt, M. S., Lowe, D. J., & Payn, T. W. (2009). Comparison of spatial prediction techniques for developing Pinus radiata productivity surfaces across New Zealand. *Forest Ecology and Management, 258*(9), 2046-2055.

Rawley, B. (2013). Implementation of the 300 Index Growth Model in YTGEN. (pp. 10).

Shiver, B. D., & Borders, B. E. (1996). Sampling techniques for forest resource inventory. [Article].

Stephens, P. R., Kimberley, M. O., Beets, P. N., Paul, T. S. H., Searles, N., Bell, A., et al. (2012). Airborne scanning LiDAR in a double sampling forest carbon inventory. *Remote Sensing of Environment, 117*, 348-357.

van der Colff, M., & Kimberley, M. O. (2013). A national height-age model for Pinus radiata in New Zealand. *New Zealand Journal of Forestry Science, 43*, 1-11.

Watt, P., Watt, M., Watt, P., & Watt, M. S. (2013). Development of a national model of Pinus radiata stand volume from lidar metrics for New Zealand. *International Journal of Remote Sensing, 34*(16), 5892-5904.